Biomaterials Science

ROYAL SOCIETY OF CHEMISTRY

PAPER

View Article Online
View Journal | View Issue

Cite this: *Biomater. Sci.*, 2021, **9**, 6957

Shape-memory balloon offering simultaneous thermo/chemotherapies to improve anti-osteosarcoma efficacy†

Sosuke Ouchi,[a,b] Eri Niiyama,[a,c] Ken Sugo,[a,c] Koichiro Uto,[a] Satoshi Takenaka,[d] Akihiko Kikuchi[b] and Mitsuhiro Ebara *[a,b,c]

This paper proposes a shape-memory balloon (SMB) to improve bone cement injection efficiency and postoperative thermo/chemotherapy for bone tumors. The SMB consists of biodegradable poly(ε-caprolactone) (PCL), an anticancer drug (doxorubicin, DOX), and heat-generating magnetic nanoparticles (MNPs). The balloon shape is fabricated in a mold by crosslinking PCL macromonomers with DOX and MNPs. The mechanical properties and shape-transition temperature (approximately 40 °C) of the SMB are modulated by adjusting the molecular weight of PCL and the crosslinking density. This allows safe inflation at the affected site with a 400% expansion rate by simple blow molding. The expanded shape is temporarily memorized at 37 °C, and the computed tomography image shows that the bone cement is successfully injected without extra pressure or leakage. The SMB releases DOX for over 4 weeks, allowing a prolonged effect at the local site. The local dosing is constant as the medication is continuously released, demonstrating an ON–OFF switchable heating/cooling response to alternating magnetic field irradiation. *In vitro* cytotoxic studies have demonstrated that heat generation/drug release and only drug release from the balloon kill approximately 99% and 60% of human osteosarcoma cells, respectively. The proposed SMB is promising in postoperative local thermo/chemotherapy for bone tumors.

Received 20th May 2021,
Accepted 4th July 2021

DOI: 10.1039/d1bm00780g

rsc.li/biomaterials-science

Introduction

Malignant bone tumors are divided into primary and metastatic tumors. The former is a rare type of cancer, which includes osteosarcoma, Ewing sarcoma, and chondrosarcoma, with an estimated 4.8 per million patients in all age groups annually.[1] For the latter, tumor cells originating in other organs are distantly metastasized; approximately 70% of patients with metastatic breast or prostate cancer develop bone metastases, and approximately 350 000 patients die each year in the United States.[2,3] Bone tumors themselves are not life-threatening; however, aggressive treatments such as preventing bone pain and fractures are required to maintain the quality of life (QOL) and to recover the locomotor apparatus, followed by postoperative therapy to prevent recurrence and metastasis.

Intramedullary nail fixation has been used to treat metastatic femoral and impending fractures, and en-bloc resection was demonstrated for primary tumors with a prosthetic replacement of the involved bone.[4,5] Conventional postoperative therapy causes serious problems such as side effects due to the systemic administration of anticancer drugs, shallow penetration of radiation, and drug and radiation resistances of tumor cells.[6] A new drug delivery system was developed using anticancer drug-incorporated bone cement to maintain high concentrations at local sites, and new hyperthermic strategies were demonstrated by generating heat using magnetic material-incorporated bone cement under an alternating magnetic field (AMF).[7,8] However, these studies did not achieve all the goals of bone tumor treatment and many required invasive surgery.

Balloon kyphoplasty (BKP) is sometimes performed as a minimally invasive treatment for the early recovery of QOL, and is a treatment method that repairs a compression-fractured vertebral body.[9] This is achieved by treating the bone tumor and osteoporosis with an inflated polyurethane balloon, followed by filling the gap with a bone cement composed of poly(methyl methacrylate). However, the disadvantages of BKP

[a]*Research Center for Functional Materials, National Institute for Materials Science (NIMS), Ibaraki 305-0044, Japan. E-mail: EBARA.Mitsuhiro@nims.go.jp*
[b]*Department of Materials Science and Technology, Tokyo University of Science, Tokyo 125-8585, Japan*
[c]*Graduate School of Pure and Applied Sciences, University of Tsukuba, Ibaraki 305-8577, Japan*
[d]*Department of Orthopaedic Surgery, Osaka International Cancer Institute, Osaka 541-8567, Japan*

†Electronic supplementary information (ESI) available. See DOI: 10.1039/d1bm00780g

include tissue damage, neuropathy, secondary fracture, and reduced QOL due to the hardening of the leaked bone cement into the spinal canal and out of the vertebral body through blood vessels.[10–12] Furthermore, iodinated contrast has been used to inflate the balloon *via* a locking syringe with a manometer for careful injection. At times, this led to bursting of the balloon and allergenic side effects due to iodine leakage.[13,14] Whereas conventional balloons for BKP are removed after expansion, under a newly developed strategy, the balloon comprising a biodegradable copolymer of D,L-lactide and ε-caprolactone was inserted in place for the injection of the bone cement.[15] Although the material could prevent bone cement leakage from the balloon, sufficient pumping pressure was required to inflate the balloon during bone cement injection. This could cause additional leakage of the bone cement, surgical difficulties, and lack of control in postoperative bone tumor therapy.

We have established a design technology for biodegradable poly(ε-caprolactone) (PCL), a Food and Drug Administration-approved biocompatible material, using shape-memory properties by introducing a crosslinked structure in the synthesis stage.[16–18] Shape-memory polymers are soft, non-invasive, and biodegradable indwelling devices as compared to metals and ceramic materials, and have been remarkably applied and commercialized in recent years. For example, a thrombectomy stent is a polyurethane-based shape-memory device that is activated by infrared laser irradiation and expands from a helical to an umbrella structure at a target site to remove thrombus in blood vessels.[19] The technique has also been applied to cranial nerve probes and ureteral stents, allowing tissue damage reduction and drug release.[20,21] PCL has also been applied to shape-memory sutures for the rapid suturing of wounds due to the shape recovery of the polymer.[22] Therefore, the development of a novel balloon for BKP using our shape-memory PCL will allow bone cement injection without extra pressure because the balloon temporarily remembers its expanded configuration. We had previously demonstrated that PCL could be easily electrospun into nanofibers incorporating magnetic nanoparticles (MNPs) and various anticancer drugs, such as doxorubicin (DOX), paclitaxel, and imiquimod, and their release properties and activities were verified.[23–25] This enabled the design of a temperature-responsive shape-memory PCL material in the presence of drugs and MNPs, which can deliver a combination of localized hyperthermia and chemotherapy by a simple ON–OFF switch for AMF. This is a promising leap for effective cancer therapeutics.[23,24]

Here we describe the design of a shape-memory balloon (SMB) for BKP, which consists of biodegradable PCL, DOX, and heat-generating MNPs, allowing a postoperative local hyperthermic chemotherapy for the treatment of bone tumors (Fig. 1).

Experimental

Materials

ε-Caprolactone, 1,4-butanediol, acryloyl chloride, and DOX were purchased from Tokyo Chemical Industry (Tokyo, Japan). Other chemicals were purchased from Tokyo Chemical Industry, Fujifilm Wako Pure Chemical (Osaka, Japan), Kanto Chemical (Tokyo, Japan), Nacalai Tesque (Kyoto, Japan), and Sigma-Aldrich (Tokyo, Japan). MNPs (γ-Fe_2O_3, <50 nm) were purchased from Sigma-Aldrich. The human osteosarcoma (HOS) cell line (RCB0992) was provided by the Riken BioResource Research Center (Ibaraki, Japan).

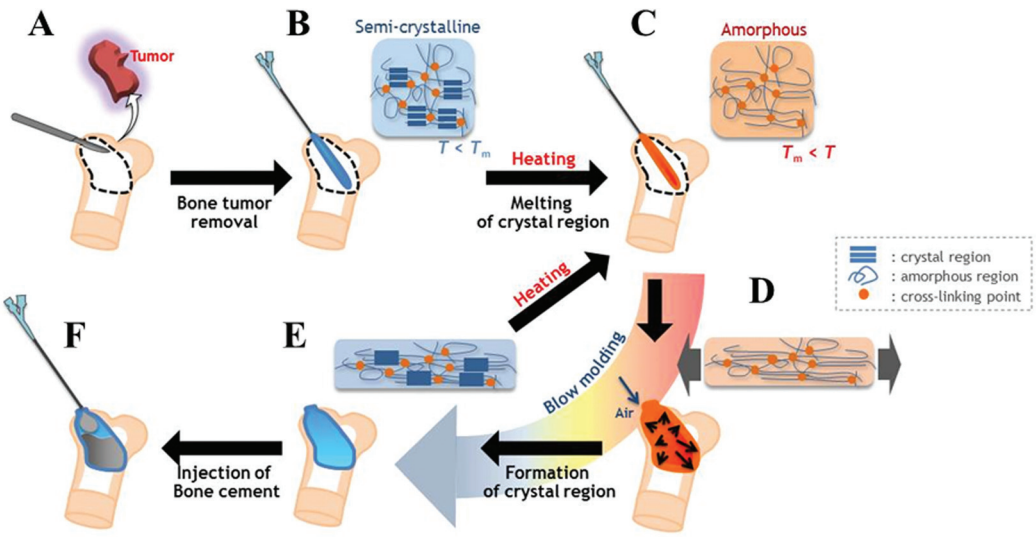

Fig. 1 Schematic illustration of the SMB as a new BKP device for bone tumor treatment. (A) Bone tumors are surgically removed. (B) The SMB is inserted. (C) Heating the SMB above its melting point causes melting of the crystalline region and phase transition to amorphous. (D) Applying expansion stress with an air blow deforms the SMB into a temporary expanded shape. (E) Cooling to body temperature re-forms the crystalline region and memorizes the temporary shape. (F) The bone cement is successfully injected without extra pressure or leakage from the SMB.

Synthesis and characterization of PCL

Fig. S1A† shows a series of synthetic reaction schemes and equations. PCL was synthesized by ring-opening polymerization from the terminal hydroxyl groups of tetramethylene glycol using tin octoate as a catalyst, by a previously reported method.[25] Briefly, 95 mL of ε-caprolactone and 1.9 mL of 1,4-butanediol were added to a round-bottomed flask under N_2 gas. Then, 30 drops of tin(II) 2-ethylhexanoate were added to the reaction flask using a micropipette. The mixed solution was allowed to react under stirring at 120 °C for 24 h. The product was completely dissolved in 300 mL of tetrahydrofuran (THF). The obtained PCL was purified by reprecipitation using 3.5 L of an equivalent mixture of hexane and diethyl ether in a yield of 96.1%. Approximately 50 g of the dried PCL was completely dissolved in 300 mL of dehydrated THF. Next, 10 mL of triethylamine and 4.7 mL of acryloyl chloride were added to the solution while stirring and ice-cooling to introduce a vinyl group at the terminal. The obtained PCL macromonomer was purified by reprecipitation by 1.5 L of methanol. The chemical structure of the obtained PCL macromonomer, including the degree of polymerization and introduction rate of the vinyl group, and the molecular weights were estimated by ^{1}H NMR (JNM-AL300, JEOL, Tokyo, Japan) and gel permeation chromatography (GPC) (JASCO International, Tokyo, Japan), respectively.

Fabrication and characteristics of SMB

The PCL macromonomer, benzoyl peroxide (BPO), DOX, MNPs, and *N*,*N*-dimethylformamide (DMF) were mixed in the following ratios: 2 wt% against PCL macromonomer for BPO; 1 or 2 wt% against solute for DOX; 0, 23.1, 33.3, and 50.0 wt% against solute for MNPs; and an equivalent amount against PCL macromonomer for DMF. The mixture was cast into a polytetrafluoroethylene (PTFE)-based mold composed of a cavity (φ 4.2 mm × h 20 mm) and a core adjusted to post-molding thicknesses of 0.3, 0.5, and 0.7 mm (Fig. S1B†). The mixture in the mold was then crosslinked and polymerized at 80 °C for 3 h (Fig. S1C†), and the volume of the resulting material was compared to that of the mold as a shrinkage rate. The resulting material was formed into a balloon shape by blow molding (N_2 flow, 0.25 MPa, 25 °C) after heating and softening above the shape-transition temperature with a hot air blower. The sizes of the obtained PCL balloon before and after expansion were measured with a caliper, and the expansion volume and expansion rate were calculated.

Bone cement injection test

For the bone cement injection test, the distal end of the porcine cadaveric femur obtained from Tokyo Shibaura Zouki (Tokyo, Japan) was drilled with a circular hole (φ 10 mm × h 20 mm), and calcium phosphate cement (Biopex-R, HOYA Technosurgical, Tokyo, Japan) was injected through an attached needle with an inner diameter of 3.7 mm into the SMB that had been blow-molded in the bone cavity. This was observed by X-ray micro-computed tomography (CT) (SKYSCAN 1272, Bruker, Kanagawa, Japan).

Characterization of SMB

To evaluate the thermal properties of the SMB, including mechanical properties, drug release, and cytotoxic activities under temperature control, the shape-memory PCL film was fabricated in the same manner as the balloon, except that a glass plate was used instead of the PTFE-based mold. The PCL film was cut into approximately 5 mg test pieces, and the amount of MNPs loaded into the PCL film was determined using a thermogravimetry-differential thermal analyzer (TG-DTA) (TG/DTA6200, Hitachi High-Tech Science, Tokyo, Japan) for a temperature range from 25 °C to 500 °C at a heating rate of 10 °C min^{-1}. The phase transition behavior, melting point, and crystallinity of the PCL film were measured by differential scanning calorimetry (DSC) (Thermo plus EVO2 DSC8231, Rigaku, Tokyo, Japan) for a temperature range from 0 °C to 100 °C at a heating rate of 5 °C min^{-1}. The crystallinity was calculated as the ratio of the melting enthalpy (ΔH_m) of the PCL film and that of a perfect PCL crystal (142 J g^{-1}):[16]

$$\text{Crystallinity}(\%) = \frac{\Delta H_m}{142} \times 100. \quad (1)$$

Mechanical properties

The mechanical properties of the PCL film under temperature control were evaluated using a table-top material tester (EZ-S, Shimadzu, Kyoto, Japan) installed in an incubation box (M-600FN, TAITEC, Saitama, Japan). PCL films (φ 16 mm × t 0.3 mm) were preincubated at 25, 31, 37, 43, and 49 °C for 60 min, and then underwent tensile testing under a crosshead speed of 5.0 mm min^{-1}, to generate a stress–strain curve for each temperature. The elastic modulus of the PCL film was calculated from the initial slope of the stress–strain curve as shown:

$$\text{Elastic modulus}(\text{MPa}) = \frac{\sigma_{\text{i.s.}}}{\varepsilon_{\text{i.s.}}} \quad (2)$$

where $\sigma_{\text{i.s.}}$ and $\varepsilon_{\text{i.s.}}$ are the stress and strain on the initial slope, respectively; the elastic modulus was plotted for each temperature.[26]

Magnetizing and heating properties

The magnetizing properties of the PCL films (φ 16 mm × t 0.3 mm) containing 0, 19.5, 31.6, and 46.1 wt% MNP determined by TG-DTA were measured using a vibrating sample magnetometer (Riken Denshi, Tokyo, Japan) to generate a magnetization curve. The heating properties of the MNP-loaded PCL films were investigated by placing the PCL films (φ 16 mm × t 0.3 mm) containing 0, 19.5, 31.6, and 46.1 wt% MNPs at the center of a customized copper coil with a diameter of 35 mm and applying an AMF (HOTSHOT2, Ambrell, Rochester, NY, USA). The heat was generated by the ON and OFF switching of the AMF (281 kHz, 4.0 V) for 360 s and 240 s, respectively, and the heating profiles were measured using a thermal imaging camera (CPA-E6, CHINO, Tokyo, Japan) every 20 s.

Drug release

To verify the drug release behavior, PCL films (φ 10 mm × t 0.3 mm) were placed one by one in a 24-well plate. Next, 2 mL of phosphate-buffered saline (PBS) was added into each well, and the plates were incubated at 37 °C for 28 days. Every 1 mL of PBS was collected on days 1, 3, 7, 14, and 28, and the equivalent volume of fresh solution was then refilled after each collection. The released DOX was detected using a fluorescence plate reader at 470 nm excitation and 550 nm emission (Infinite 200 Pro M Nano$^+$, Tecan Japan, Kanagawa, Japan). The cumulative amount of the released DOX was calculated as follows:

$$w_n = w_{n-1} + \left(C_n \times l - \frac{C_{n-1} \times l}{2}\right) \quad (3)$$

where w_n (μg) and C_n (μg mL^{-1}) are the cumulative release amount and concentration of DOX at the n^{th} (n = 1, 3, 7, 14, and 28) collection day, respectively, and l is the volume of PBS (2 mL).

Cell preparation

HOS cells were used in this study. The growth medium was the minimum essential medium of Earle's salt, which was supplemented with 0.1 mM non-essential amino acid, 10% (v/v) fetal bovine serum, and 1% (v/v) penicillin–streptomycin. HOS cells were prepared by subcultures in tissue culture dishes (100 mm) after two days of incubation at 37 °C in 5% CO_2 (MCO-170AICUVH, PHC Holdings, Tokyo, Japan). The cells were collected with 0.25% (w/v) trypsin-1 mM ethylenediaminetetraacetic acid from the confluent monolayer in the dish and then resuspended in 12 mL of the growth medium for subsequent experiments.

Thermal and drug sensitivity of HOS cells

A volume of 0.2 mL of each cell suspension prepared in advance at 2.45 × 10^5 cells mL^{-1} was seeded on a 96-well plate and cultured for 48 h, before the addition of the DOX and adjusted to concentrations of 0, 0.2, 0.4, 0.6, 0.8, 2, 6, 8, 10, 20, and 40 μg mL^{-1} in the growth medium. They were prepared in two groups, and one was preincubated at 45 °C in 5% CO_2 for 60 min. Then, all test specimens were cultured for another 24 h at 37 °C in 5% CO_2. The Alamar blue assay reagent (10% against medium) was then added to each well and the plates were incubated for 2.5 h at 37 °C, according to the protocol.[27] The cell number was calculated from the fluorescence intensity measured using a fluorescence plate reader at 570 nm excitation and 600 nm emission (Tecan, Japan). The cell viability and IC_{50} were calculated based on the cell number in the control group (0 μg mL^{-1} DOX) at a viability of 100%.

AMF-responsive cytotoxic activity *in vitro*

A volume of 2 mL of each cell suspension prepared in advance at 2.45 × 10^4 cells mL^{-1} was seeded on a 6-well plate and cultured for 48 h, before co-culturing with PCL films (φ 10 mm × t 0.3 mm), and labeled as MNPs_Film (PCL film with 31.6 wt% MNPs without DOX) and MNPs/DOX_Film (PCL film with 31.6 wt% MNPs and 2.0 wt% DOX). Additionally, both groups were exposed to AMF irradiation (281 kHz, 4.0 V) for 60 min and were labeled as MNPs_Film (AMF) and MNPs/DOX_Film (AMF), respectively. All test specimens were cultured for another 24 h at 37 °C in 5% CO_2. The cell number and viability were calculated in the same manner as described above and were based on the cell number in the control group (growth medium only) at a viability of 100%.

Statistical analysis

All data were expressed as a mean and standard deviation (mean ± SD) in triplicate. Statistical analyses were performed using the Microsoft Excel 2019 software (Microsoft, Redmond, WA, USA). The cell viability was statistically compared using an unpaired t-test, and differences were considered significant if p-values were less than 0.05.

Results

Characterization of PCL

The structure of the obtained PCL macromonomer was confirmed by ^{1}H NMR spectroscopy (Fig. S2 and S3†). The chemical shifts were: ^{1}H NMR, δ ($CDCl_3$, ppm); 1.40 (m, 2H, –$COCH_2CH_2CH_2CH_2CH_2O$–), 1.65 (m, 4H, –$COCH_2CH_2CH_2CH_2CH_2O$–), 2.31 (t, 2H, –$COCH_2CH_2CH_2CH_2CH_2O$–), 4.06 (t, 2H, –$COCH_2CH_2CH_2CH_2CH_2O$–), and 5.85, 6.12, and 6.40 (m, 3H, –CH=CH_2). The average degree of polymerization and the percentage of introduction of a vinyl group were estimated to be 19.8 and 91.3%, respectively. The molecular weight of the obtained PCL macromonomer was determined by GPC and estimated to be approximately 4900.

Shape-memory properties

The shape-memory PCL film, as a simple alternative, was used to verify the characteristics of the SMB. Fig. 2A shows the melting (shape transition) temperature of each test specimen compared *via* DSC analysis, indicating that the melting points of the crosslinked PCL films with and without MNP loading were 42.1 °C and 39.4 °C, respectively, while those of the PCL and PCL macromonomer before crosslinking were 53.9 °C and 53.4 °C, respectively. This demonstrated the successful fabrication of a crosslinked PCL film with a shape-transition temperature of approximately 40 °C, which is close to the human body temperature.

Fig. 2B depicts the shape-memory properties using the PCL film. The left side of Fig. 2B shows the original piece of PCL film (t = 0.3 mm) at room temperature. Subsequently, as shown on the right side of Fig. 2B, applying tensile stress above the shape-transition temperature caused deformation of the PCL film, followed by crystallization, and fixation of the shape by cooling below 37 °C. This shape-memory property can be applied to balloon-shaped materials such as those fabricated in this study. Blow molding could easily expand the SMB above its shape-transition temperature, and the inflated

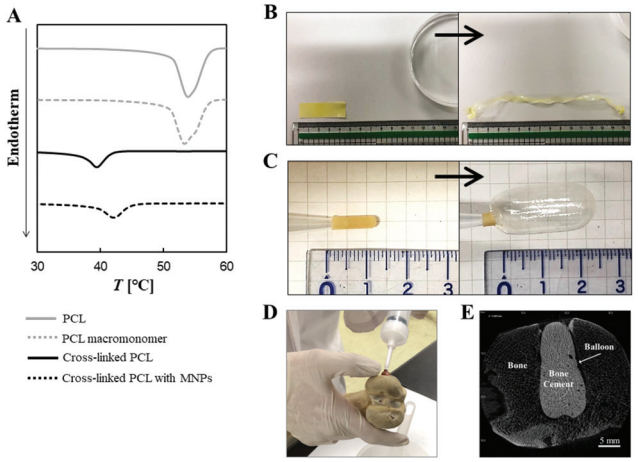

Fig. 2 Shape-memory properties of the SMB at approximately the shape-transition temperature. (A) Melting (shape transition) temperature of each test specimen by DSC. (B) Shape-memory property of an original piece of shape-memory PCL film. Applying tensile stress above the shape-transition temperature deformed the material and memorized its shape by cooling to room temperature, as shown in the left to right. (C) Shape-memory property of the fabricated SMB. Blow molding above the shape-transition temperature expanded the SMB and memorized its shape by cooling below 37 °C, as shown in the left to right. (D) Injection process and (E) CT image in bone cement injection test. (C)–(E) show the result of SMB with a thickness of 0.3 mm.

shape was memorized by cooling below 37 °C (Fig. 2C). Three types of SMB with different thicknesses were designed by modifying the diameter of the mold core, and all the SMBs were successfully fabricated with a 74.8% shrinkage, regardless of the MNP loading (Fig. S4†). Table 1 shows the expansion pressure, expansion volume, and expansion rate for each balloon thickness, especially accomplishing around 400% expansion. Table 2 shows the melting enthalpy and the crystallinity of each test specimen. The melting enthalpy was calculated as the integral of the DSC curve, shown in Fig. 2A, from 20 °C to 80 °C. The introduction of a crosslinking structure into the PCL chain lowered the crystallinity of the PCL film and allowed free control of the shape-transition temperature.

Fig. 2D and E show the injection process and CT image in the bone cement injection test, respectively. The bone cement was successfully injected without extra pressure or balloon leakage.

Table 1 Geometry characteristics of SMB before and after blow molding

Thickness of the balloon [mm]	Expansion pressure [MPa]	Expansion volume [mL]	Expansion rate [%]
t = 0.30	0.20	3.88	392
t = 0.50	0.30	4.02	402
t = 0.70	0.30	4.32	412

Table 2 Characteristics of each test specimen, including melting point (T_m), melting enthalpy (ΔH_m), and crystallinity

	T_m [°C]	ΔH_m [J g^{-1}]	Crystallinity [%]
PCL	53.9	74.1	52.2
PCL macromonomer	53.4	77.3	54.4
Cross-linked PCL	39.4	52.6	37.0
Cross-linked PCL with MNPs	42.1	55.3	38.9

Characterization and mechanical properties of SMB

PCL films prepared with 0, 23.1, 33.3, and 50.0 wt% MNP loading contained 0, 19.5, 31.6, and 46.1 wt% MNPs, respectively, which were identified by TG-DTA analysis as the weight of residual materials at 500 °C (Fig. S5†). The result indicated that there was no significant loss in the MNPs during the fabrication process, which will allow the achievement of the expected material design.

Fig. 3A shows the stress–strain curve of the PCL film under controlled temperature. Yield stresses were observed at 25, 31, and 37 °C, whereas no yield points were found at 43 °C and 49 °C. Fig. 3B shows the elastic modulus of the PCL film at each temperature, indicating a gradual decrease with increasing temperature. However, the modulus decreased markedly from 37 °C to 43 °C, which was similar to the shape-transition temperature range of the crosslinked PCL film shown in Fig. 2A.

Magnetizing properties and heat generation

Fig. 4A shows the magnetization curve of the PCL films containing 0, 19.5, 31.6, and 46.1 wt% MNP. The loading amount of MNPs increased the saturation flux density but did not affect the material-dependent coercivity, which resulted in heat generation during AMF irradiation. Fig. 4B and C show the infrared thermal images of the PCL film containing 31.6 wt% MNP after AMF irradiation for 360 s. This indicates a uniform exotherm within the film, compared to that of the PCL film without MNP loading (Fig. S6†). Fig. 4D shows the time-dependent temperature changes in PCL films for different MNP loading rates under AMF irradiation for 360 s.

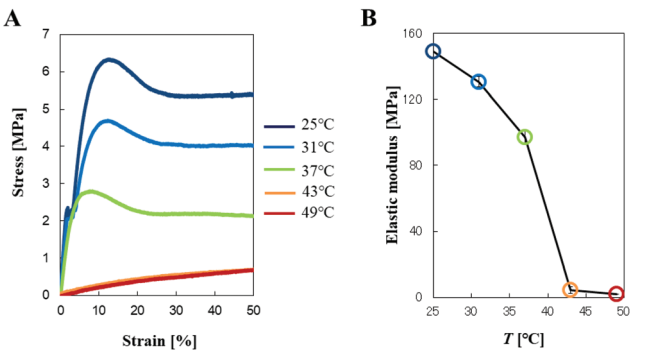

Fig. 3 Mechanical properties of the PCL film, as a simple alternative to the SMB, under temperature control. (A) Stress–strain curve and (B) elastic modulus of the PCL film at each temperature, which was calculated from the initial slope of the stress–strain curve shown in A.

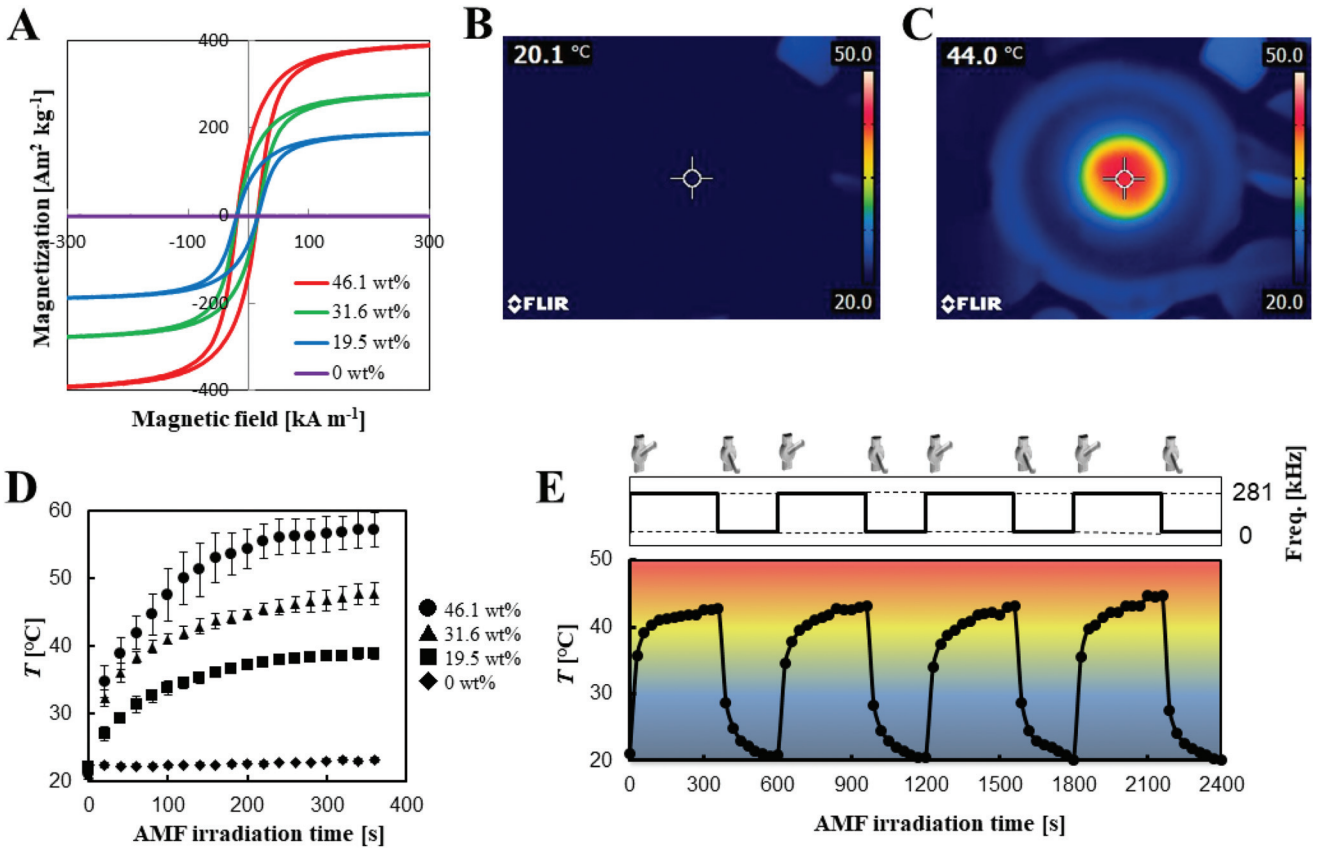

Fig. 4 Magnetizing properties and heat generation by ON–OFF switching of AMF irradiation. (A) Magnetization curve of PCL films containing 0, 19.5, 31.6, and 46.1 wt% MNP measured using a vibrating sample magnetometer; infrared thermal images of the PCL film containing 31.6 wt% MNP at (B) 0 s and (C) 360 s after AMF irradiation; (D) time-dependent temperature changes of PCL films at different MNP contents: 0, 19.5, 31.6, and 46.1 wt%, under AMF irradiation for 360 s; (E) heating profiles of the PCL film containing 31.6 wt% MNP by ON–OFF switching of the AMF irradiation (ON for 360 s and OFF for 240 s).

The temperature of each test specimen sharply increased immediately after AMF irradiation and reached a plateau within a few minutes at 38.9, 47.8, and 57.0 °C in the PCL films containing 19.5, 31.6, and 46.1 wt% MNP, respectively. The results indicated that the heating profiles are dependent on the AMF power, coil diameter, and the concentration of MNP loading, which allow better control over the heat generation of SMB. Fig. 4E shows the heating profiles of the PCL film containing 31.6 wt% MNP and a 600 s ON–OFF switching AMF cycle (ON for 360 s and OFF for 240 s). The temperature of the PCL film rose above 43 °C within a few minutes upon irradiation of 281 kHz AMF and dropped sharply to 25 °C once the irradiation was turned off. Furthermore, heat generation was reproduced upon repeated ON–OFF switching of the AMF.

Drug release

In this study, PCL films containing DOX (1.0 or 2.0 wt%) and MNPs (0 or 31.6 wt%) were used to verify the drug release behavior of SMB. Fig. 5 shows the cumulative amount of DOX released by the PCL films. Each test specimen released DOX gradually after an initial burst and showed a sustained release over 28 days. The release of DOX increased depending on the additive DOX amount, whereas that of the group with MNP loading was markedly suppressed. The drug release efficiencies until the 28th day were 75.8%, 64.0%, 4.89%, and 2.45% for the samples with 2.0 wt% DOX, 1.0 wt% DOX, 2.0 wt%

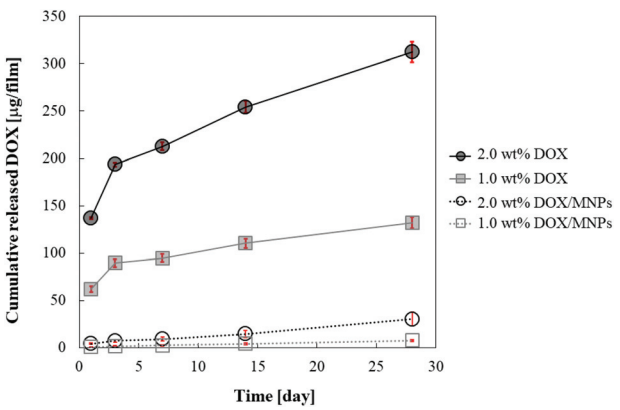

Fig. 5 Cumulative amount of DOX released from PCL films containing DOX (1.0 and 2.0 wt%) and MNPs (0 wt% and 31.6 wt%). The experiment was performed at 37 °C for a period of 28 days.

DOX/MNPs, and 1.0 wt% DOX/MNPs, respectively. The initial feed amount of DOX in the film was considered to be the total loading content (100%) in this study because we did not conduct a washing process.

Cytotoxic effect

Fig. 6A shows the viability of HOS cells after DOX treatment with and without pre-incubation at 45 °C for 60 min. The IC_{50} values of DOX with and without pre-incubation were 0.40–0.80 and 2.0–8.0 μg mL^{-1}, respectively, indicating that the viabilities of HOS cells decreased depending on the concentration of DOX and were sensitive to temperature.

In contrast, HOS cells and PCL films were co-cultured for 24 h with and without AMF irradiation. There was a significant reduction in the cell viability between MNPs/DOX_Film (PCL film with 31.6 wt% MNPs and 2.0 wt% DOX) and MNPs/DOX_Film (AMF) (PCL film with 31.6 wt% MNPs and 2.0 wt% DOX irradiated with AMF), to 40.3% and 1.02%, respectively (Fig. 6B). Furthermore, MNPs_Film (AMF) (PCL film with 31.6 wt% MNPs without DOX irradiated with AMF) showed a significant reduction of 1.32% in the cell viability. The result indicated that DOX released from the PCL film showed a killing effect of approximately 60% on the HOS cells, which might be increased to approximately 99% upon heating of the MNPs by AMF irradiation. However, there was no significant difference between MNP_Film (AMF) and MNPs/DOX_Film (AMF), suggestive of the high heat sensitivity property of the HOS cells used in this study.

Discussion

In this study, we designed a strategy of a new BKP system for bone tumor treatment using the SMB with the following features: heating the SMB above its melting point causes melting of the crystalline region and phase transition to amorphous, applying expansion stress with an air blower deforms the SMB into a temporary expanded shape, cooling to body temperature re-forms the crystalline region and memorizes the temporary shape, and the bone cement is successfully injected without extra pressure or leakage from the SMB. Furthermore, the SMB consists of biodegradable PCL, an anticancer drug DOX, and heat-generating MNPs, promising postoperative thermo/chemotherapy without removing it from the affected site. Next, we developed an SMB with a shape-transition temperature of approximately 40 °C (near body temperature), which contributes to the shape change and primary shape-memory of the balloon at biosafety temperatures, allowing safe balloon expansion and bone cement injection at the affected site (Fig. 2A and C, and Table 2). The obtained balloon achieved an expansion rate of approximately 400% by simple blow molding under an expansion pressure of 0.2–0.3 MPa, depending on the balloon thickness (Table 1). The expanded shape was temporarily memorized, regardless of the MNP loading and film thickness; therefore, the bone cement was successfully injected without extra pressure or leakage from the balloon (Fig. 2D and E). A conventional polyurethane balloon for BKP required a maximum expansion pressure of 2.7 MPa to obtain an expansion volume of 4 mL due to its high elasticity, indicating an expansion rate of approximately 100% and a 10-fold expansion pressure for the same expansion volume as the SMB.[28] This leads to a high risk of balloon burst. Furthermore, the SMB would gradually lead to osteogenesis of the bone cement with the biodegradation of PCL, which depends on the crosslinking and molecular weight of PCL. This area of research requires further examination.

To overcome recurrence, metastasis, and fracture reduction in the treatment of bone tumors, the SMB was designed to simultaneously offer thermal properties with drug release. Hyperthermia is a traditional method of cancer therapy as cancer cells are more sensitive to heat than normal cells.[29] Currently, local hyperthermia with an AMF has been developed using MNPs as a heating element, which rapidly heats due to hysteresis loss caused by the AMF that can reach the depths of the human body.[8,30] Therefore, the heat generation behavior of the PCL film with MNP loading was verified to be an alternative to that of the SMB. The MNPs used in this study were iron oxide (γ-Fe_2O_3) nanoparticles with a diameter <50 nm. The saturation flux density increased with the increasing loading of MNPs (Fig. 4A). The temperature of the PCL film containing 31.6 wt% MNP increased above 43 °C, an effective hyperthermic temperature, within a few minutes after AMF irradiation, showing a uniform exotherm within the film (Fig. 4B–D). Heat generation was reproduced by repeated ON–OFF switching of the AMF. The AMF power, coil diameter, and concentration of MNP loading also affected the heat generation (Fig. 4D and E). This made the heat generation of the SMB more controllable. For radiofrequency treatment, general hyperthermia, it is difficult to heat the target site without damaging normal tissue until the intended temperature has been achieved upon adjusting to a narrow temperature range of 42–45 °C.[29,31] The treatments last for 40–60 min and the intratumor temperature reaches its maximum in 10–15 min.[32,33] Prolonged heating of

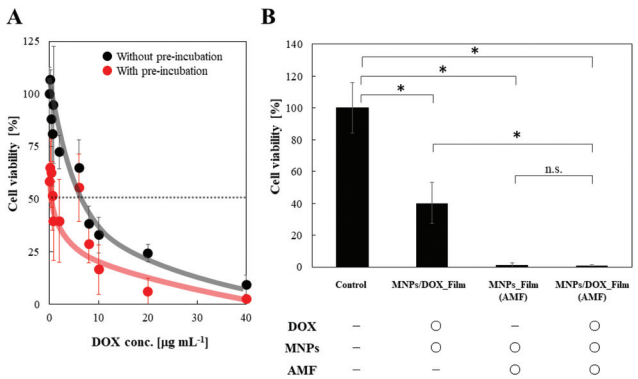

Fig. 6 Cytotoxic effects of DOX release and heat generation on HOS cells. (A) Viability of HOS cells by DOX treatment with and without pre-incubation at 45 °C and (B) viability of HOS cells by DOX release from the PCL film and/or heating generation by AMF irradiation (n = 3; *, p < 0.05; n.s., not significant).

the intratumor causes dehydration, sweating, and skin pain in patients. The SMB locally heats the target site and reaches the maximum temperature within 5 min after AMF irradiation (Fig. 4D and E), which could reduce the burden of hyperthermia. Hyperthermia by near-infrared light irradiation was demonstrated using gold and magnetite nanoparticles; however, near-infrared light does not reach deep inside the bone due to its low penetrability and penetrates only a few millimeters from the body surface, as compared to the AMF irradiation used in this study.[34–37] Near-infrared rays that reached deep inside the body were detected using an endoscope.[37] This method is a burden for the patient during each hyperthermia treatment. Unlike the previously mentioned method, using the SMB with MNP loading is a minimally invasive approach, and the SMB can be placed directly at the surgical site, resulting in good thermal accumulation on the tumor.[24]

To verify the drug release behavior of SMB, DOX was used in this study, which is a common chemotherapeutic drug with a wide anti-tumor spectrum that is not limited to bone tumors.[38,39] Each PCL film continued to gradually release DOX after the initial burst, showing a sustained release over 28 days (Fig. 5). This drug release phenomenon is based on the permeation of DOX in the PCL film. Moreover, a larger amount of DOX could permeate and release through the PCL film above the shape-transition temperature.[18] The temperature-responsive drug release is triggered by the self-heating of MNPs by AMF irradiation in our method. The release of DOX increased depending on the additive amount, whereas that of the group with MNP loading was markedly suppressed (Fig. 5). This result was considered to be a drug–material interaction between the $-NH_2$ and –OH groups of DOX with the –OH groups present on the hydrated surface of iron oxide through hydrogen bonding.[40] DOX and MNPs are key materials in the described strategy. Therefore, it is important to verify whether DOX shows cytotoxic effects with a suppressed release in the presence of MNPs. This was verified by screening with HOS cells as discussed below.

Fig. 6A shows the cytotoxic effect of DOX and heat treatment on the HOS cells. The cell viability decreased depending on the concentration of DOX, and the IC_{50} values of DOX with and without pre-incubation at 45 °C for 60 min were 0.40–0.80 and 2.0–8.0 μg mL^{-1}, respectively. The results indicated that HOS cells are heat-sensitive, and that heat treatment may have a synergistic effect with DOX.

HOS cells and PCL films were then co-cultured for 24 h, and the cytotoxic effect on HOS cells was verified using the method mentioned above. However, the heat generation was induced by self-heating of MNPs by AMF irradiation for 60 min (Fig. 6B). The cell viabilities by DOX release and heat generation were 40.3 and 1.32%, respectively, indicating that each treatment had a significant cytotoxic effect on HOS cells. Although the release of DOX, as shown in Fig. 5, was markedly suppressed in the presence of MNPs, this *in vitro* test using HOS cells and the PCL film revealed that even a low amount of DOX release could exhibit sufficient cytotoxic effect on HOS cells. The combination of DOX release and heat generation showed a superior cytotoxic effect (1.02% viability), indicating that DOX release from the PCL film had a killing effect of approximately 60% on HOS cells, which could be enhanced to approximately 99% with heat generation of MNPs by AMF irradiation. However, the combined treatment showed no significant difference when compared to the heat generation treatment (1.32% viability). The results indicated that the HOS cells used in this study were more sensitive to heat than DOX. AMF irradiation for 60 min or less would be extremely effective for postoperative bone tumor treatment using the SMB. Current hyperthermia requires more time to warm bone tumors deep inside the body, due to the low thermal conductivity and thickness of the cortical bone.[8,33] Therefore, the development and optimization of an *in vivo* model will be needed to observe the synergistic thermo/chemo effects in the future.

Conclusions

We described the design of an SMB with a shape-transition temperature of approximately 40 °C (near body temperature), fabricated by crosslinking PCL macromonomers in the presence of DOX and MNPs. It allowed safe balloon inflation at the affected site with a 400% expansion rate by simple blow molding. The expanded shape was temporarily memorized at 37 °C, and the bone cement was successfully injected without extra pressure and leakage from the balloon. The PCL film, as a simple alternative to the SMB, could be locally heated by ON–OFF switching of the AMF irradiation. It reached an effective hyperthermia temperature (42–45 °C) within 5 min, and released DOX for over four weeks, allowing a prolonged effect at the local site as the continuous release of medication kept the local drug concentration constant. *In vitro* cytotoxic studies demonstrated that a combined heat generation and drug release and another experiment with only drug release killed approximately 99 and 60% of HOS cells, respectively. The proposed SMB is promising in postoperative local hyperthermic chemotherapy for the treatment of bone tumors.

Conflicts of interest

There are no conflicts to declare.

Acknowledgements

This work was financially supported by JSPS KAKENHI Grant-in-Aid for Scientific Research (B) (JP19H04476) and Grant-in-Aid for Transformative Research Areas (A) (JP20H05877).

Notes and references

1 I. W. Folkert, S. Devalaraja, G. P. Linette, K. Weber and M. Haldar, *J. Bone Miner. Res.*, 2019, **34**, 1780–1788.
2 D. Bhowmik, X. Song, M. Intorcia, S. Gray and N. Shi, *Curr. Med. Res. Opin.*, 2019, **35**, 513–523.

3 J. F. Huang, J. Shen, X. Li, R. Rengan, N. Silvestris, M. Wang, L. Derosa, X. Zheng, A. Belli, X. L. Zhang, Y. M. Li and A. Wu, *Ann. Transl. Med.*, 2020, **8**, 482, DOI: 10.21037/atm.2020.03.55.
4 S. A. Barwood, J. L. Wilson, R. R. Molnar and P. F. Choong, *Acta Orthop. Scand.*, 2000, **71**, 147–152.
5 G. Rosen, M. L. Murphy, A. G. Huvos, M. Gutierrez and R. C. Marcove, *Cancer*, 1976, **37**, 1–11.
6 H. T. Ta, C. R. Dass, P. F. M. Choong and D. E. Dunstan, *Cancer Metastasis Rev.*, 2009, **28**, 247–263.
7 Y. Tanzawa, H. Tsuchiya, T. Shirai, H. Nishida, K. Hayashi, A. Takeuchi, M. Kawahara and K. Tomita, *J. Orthop. Sci.*, 2011, **16**, 77–84.
8 A. Matsumine, K. Takegami, K. Asanuma, T. Matsubara, T. Nakamura, A. Uchida and A. Sudo, *Int. J. Clin. Oncol.*, 2011, **16**, 101–108.
9 S. R. Garfin, H. A. Yuan and M. A. Reiley, *Spine*, 2001, **26**, 1511–1515.
10 T. Kobayashi, Y. Arai, Y. Takeuchi, Y. Nakajima, Y. Shioyama, M. Sone, N. Tanigawa, O. Matsui, M. Kadoya and Y. Inaba, *Ann. Oncol.*, 2009, **20**, 1943–1947.
11 T. J. Kaufmann, M. E. Jensen, G. Ford, L. L. Gill, W. F. Marx and D. F. Kallmes, *Am. J. Neuroradiol.*, 2002, **23**, 601–604.
12 I. J. Lee, A. L. Choi, M. Y. Yie, J. Y. Yoon, E. Y. Jeon, S. H. Koh, D. Y. Yoon, K. J. Lim and H. J. Im, *Acta Radiol.*, 2010, **51**, 649–654.
13 H. Hameed, M. Hameed and S. P. Cohen, *Essential of Pain Medicine*, Elsevier, Amsterdam, 4th edn, 2018.
14 S. Becker, *Balloon Kyphoplasty*, Springer Nature, London, 2008.
15 X. Liu, D. Wei, J. Zhong, M. Ma, J. Zhou, X. Peng, Y. Ye, G. Sun and D. He, *ACS Appl. Mater. Interfaces*, 2015, **7**, 18540–18552.
16 M. Ebara, K. Uto, N. Idota, J. M. Hoffman and T. Aoyagi, *Adv. Mater.*, 2012, **24**, 273–278.
17 Q. Shou, K. Uto, M. Iwanaga, M. Ebara and T. Aoyagi, *Polym. J.*, 2014, **46**, 492–498.
18 K. Uto, K. Yamamoto, S. Hirase and T. Aoyagi, *J. Controlled Release*, 2006, **110**, 408–413.
19 G. M. Baer, W. Small, T. S. Wilson, W. J. Benett, D. L. Matthews, J. Hartman and D. J. Maitland, *Biomed. Eng. OnLine*, 2007, **6**, 43, DOI: 10.1186/1475-925X-6-43.
20 A. A. Sharp, H. V. Panchawagh, A. Ortega, R. Artale, S. Richardson-Burns, D. S. Finch, K. Gall, R. L. Mahajan and D. Restrepo, *J. Neural Eng.*, 2006, **3**, L23–L30.
21 A. T. Neffe, B. D. Hanh, S. Steuer and A. Lendlein, *Adv. Mater.*, 2009, **21**, 3394–3398.
22 A. Lendlein and R. Langer, *Science*, 2002, **296**, 1673.
23 Y. J. Kim, M. Ebara and T. Aoyagi, *Adv. Funct. Mater.*, 2013, **23**, 5753–5761.
24 E. Niiyama, K. Uto, C. M. Lee, K. Sakura and M. Ebara, *Adv. Healthcare Mater.*, 2019, **8**, e1900102, DOI: 10.1002/adhm.201900102.
25 R. Garrett, E. Niiyama, Y. Kotsuchibashi, K. Uto and M. Ebara, *Fibers*, 2015, **3**, 478–490.
26 A. Lendlein and S. Kelch, *Angew. Chem., Int. Ed.*, 2002, **41**, 2034–2057.
27 S. A. Ahmed, R. M. Gogal Jr. and J. E. Walsh, *J. Immunol. Methods*, 1994, **170**, 211–224.
28 K. Zapałowicz and M. Radek, *Neurol. Neurochir. Pol.*, 2015, **49**, 11–15.
29 B. V. Harmon, A. M. Corder, R. J. Collins, G. C. Gobé, J. Allen, D. J. Allan and J. F. Kerr, *Int. J. Radiat. Biol.*, 1990, **58**, 845–858.
30 H. Mamiya and B. Jeyadevan, *Sci. Rep.*, 2011, **1**, 157, DOI: 10.1038/srep00157.
31 A. Ito, M. Shinkai, H. Honda, K. Yoshikawa, S. Saga, T. Wakabayashi, J. Yoshida and T. Kobayashi, *Cancer Immunol. Immunother.*, 2003, **52**, 80–88.
32 K. D. Paulsen, J. W. Strohbehn, S. C. Hill, D. R. Lynch and F. E. Kennedy, *Int. J. Radiat. Oncol., Biol., Phys.*, 1984, **10**, 1095–1107.
33 M. Abe, M. Hiraoka, M. Takahashi, S. Egawa, C. Matsuda, Y. Onoyama, K. Morita, M. Kakehi and T. Sugahara, *Cancer*, 1986, **58**, 1589–1595.
34 V. De Matteis, M. Cascione, C. C. Toma and R. Rinaldi, *Curr. Pharm. Des.*, 2019, **25**, 1477–1489.
35 M. Chu, Y. Shao, J. Peng, X. Dai, H. Li, Q. Wu and D. Shi, *Biomaterials*, 2013, **34**, 4078–4088.
36 V. Ntziachristos, C. Bremer and R. Weissleder, *Eur. Radiol.*, 2003, **13**, 195–208.
37 H. Kobayashi and P. L. Choyke, *Acc. Chem. Res.*, 2019, **52**, 2332–2339.
38 D. Zhao, H. Yuan, F. Yi, C. Meng and Q. Zhu, *Mol. Med. Rep.*, 2014, **9**, 1975–1981.
39 P. A. Speth, Q. G. van Hoesel and C. Haanen, *Clin. Pharmacokinet.*, 1988, **15**, 15–31.
40 S. Kayal and R. V. Ramanujan, *Mater. Sci. Eng., C*, 2010, **30**, 484–490.